J|A|C|S
ARTICLES
Published on Web 12/10/2006

Proton-Coupled Electron Transfer in Soybean Lipoxygenase: Dynamical Behavior and Temperature Dependence of Kinetic Isotope Effects

Elizabeth Hatcher, Alexander V. Soudackov, and Sharon Hammes-Schiffer*

Contribution from the Department of Chemistry, 104 Chemistry Building, Pennsylvania State University, University Park, Pennsylvania 16802

Received September 18, 2006; E-mail: shs@chem.psu.edu

Abstract: The dynamical behavior and the temperature dependence of the kinetic isotope effects (KIEs) are examined for the proton-coupled electron transfer reaction catalyzed by the enzyme soybean lipoxygenase. The calculations are based on a vibronically nonadiabatic formulation that includes the quantum mechanical effects of the active electrons and the transferring proton, as well as the motions of all atoms in the complete solvated enzyme system. The rate constant is represented by the time integral of a probability flux correlation function that depends on the vibronic coupling and on time correlation functions of the energy gap and the proton donor−acceptor mode, which can be calculated from classical molecular dynamics simulations of the entire system. The dynamical behavior of the probability flux correlation function is dominated by the equilibrium protein and solvent motions and is not significantly influenced by the proton donor−acceptor motion. The magnitude of the overall rate is strongly influenced by the proton donor−acceptor frequency, the vibronic coupling, and the protein/solvent reorganization energy. The calculations reproduce the experimentally observed magnitude and temperature dependence of the KIE for the soybean lipoxygenase reaction without fitting any parameters directly to the experimental kinetic data. The temperature dependence of the KIE is determined predominantly by the proton donor−acceptor frequency and the distance dependence of the vibronic couplings for hydrogen and deuterium. The ratio of the overlaps of the hydrogen and deuterium vibrational wavefunctions strongly impacts the magnitude of the KIE but does not significantly influence its temperature dependence. For this enzyme reaction, the large magnitude of the KIE arises mainly from the dominance of tunneling between the ground vibronic states and the relatively large ratio of the overlaps between the corresponding hydrogen and deuterium vibrational wavefunctions. The weak temperature dependence of the KIE is due in part to the dominance of the local component of the proton donor−acceptor motion.

I. Introduction

Lipoxygenase is a non-heme iron metalloenzyme that catalyzes the oxidation of unsaturated fatty acids. The human form is medically significant because it assists in the production of leukotrienes and lipoxins, which play a role in immune response.[1] Moreover, the inhibition of lipoxygenase has been found to aid in the prevention of cancer.[2−5] Kinetic studies have been conducted for human lipoxygenase[6,7] and soybean lipoxygenase-1 (SLO)[8,9] with linoleic acid, the natural substrate for SLO. High-resolution crystal structures have been solved for SLO.[10,11] In addition, a number of mutants of SLO have been studied experimentally.[9,11,12]

The hydrogen abstraction step of the reaction catalyzed by SLO is depicted in Figure 1. In this step of the catalytic reaction, the pro-*S* hydrogen from the C11 carbon of the linoleic acid substrate is abstracted by the Fe(III)-OH cofactor to form a radical intermediate substrate and Fe(II)-OH_2. Subsequently, the radical form of the linoleic acid reacts with dioxygen to ultimately form hydroperoxyoctadecadienoic acid and the ferric form of the iron cofactor. Quantum mechanical calculations[13] suggest that the hydrogen abstraction step occurs by a proton-coupled electron transfer (PCET) mechanism, in which the electron transfers from the π-system of the substrate to the iron of the cofactor, while the proton transfers from the C11 carbon of the substrate to the hydroxyl ligand of the cofactor. Moreover,

(1) Samuelsson, B.; Dahlen, S.-E.; Lindgren, J. A.; Rouzer, C. A.; Serhan, C. N. *Science* **1987**, *237*, 1171−1176.
(2) Steele, V. E.; Holmes, C. A.; Hawk, E. T.; Kopelovich, L.; Lubet, R. A.; Crowell, J. A.; Sigman, C. C.; Kelloff, G. J. *Cancer, Epidemiol., Biomarkers Prev.* **1999**, *8*, 467−483.
(3) Rioux, N.; Castonguay, A. *Carcinogenesis* **1998**, *19*, 1393−1400.
(4) Nie, D.; Hillman, G. G.; Geddes, T.; Tang, K.; Pierson, C.; Grignon, D. J.; Honn, K. V. *Cancer Res.* **1998**, *58*, 4047−4051.
(5) Ghosh, J.; Myers, C. E. *Proc. Natl. Acad. Sci. U.S.A.* **1998**, *95*, 13182−13187.
(6) Lewis, E. R.; Johansen, E.; Holman, T. R. *J. Am. Chem. Soc.* **1999**, *121*, 1395−1396.
(7) Segraves, E. N.; Holman, T. R. *Biochemistry* **2003**, *42*, 5236−5243.
(8) Rickert, K. W.; Klinman, J. P. *Biochemistry* **1999**, *38*, 12218−12228.
(9) Knapp, M. J.; Rickert, K. W.; Klinman, J. P. *J. Am. Chem. Soc.* **2002**, *124*, 3865−3874.
(10) Minor, W.; Steczko, J.; Stec, B.; Otwinowski, Z.; Bolin, J. T.; Walter, R.; Axelrod, B. *Biochemistry* **1996**, *35*, 10687−10701.
(11) Tomchick, D. R.; Phan, P.; Cymborowski, M.; Minor, W.; Holman, T. R. *Biochemistry* **2001**, *40*, 7509−7517.
(12) Knapp, M. J.; Seebeck, F. P.; Klinman, J. P. *J. Am. Chem. Soc.* **2001**, *123*, 2931−2932.
(13) Lehnert, N.; Solomon, E. I. *J. Biol. Inorg. Chem.* **2003**, *8*, 294−305.

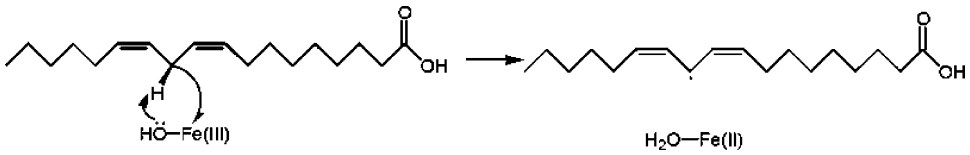

Figure 1. Hydrogen abstraction step of the reaction catalyzed by soybean lipoxygenase with its natural substrate linoleic acid. In this step, a hydrogen is abstracted from the linoleic acid to the iron cofactor.

analysis of the thermodynamic properties of the single proton transfer and electron transfer reactions, as well as the concerted PCET mechanism, indicates that the single proton transfer and electron transfer reactions are highly endothermic, whereas the PCET reaction is exothermic.[9,14] Thus, the electron and proton transfer simultaneously to avoid the high-energy intermediates.

Klinman and co-workers determined that the hydrogen abstraction step in the SLO reaction is rate limiting above 32 °C.[9] The deuterium kinetic isotope effect (KIE) of this reaction was observed to be unusually high, with a value of 81 at room temperature,[8,9,15−17] and the temperature dependences of the rates and KIEs were found to be relatively weak.[9] Moreover, human lipoxygenase was observed to behave similarly.[6,7] This behavior was interpreted to indicate that hydrogen tunneling, as well as a vibrational promoting mode, play important roles in these enzymatic reactions.[9,14] These intriguing results have stimulated extensive theoretical activity.

The SLO reaction has been studied with density functional theory[13,18−20] and various quantum/classical approaches.[8,9,14,17,21−27] Most of these theoretical studies were based on simple models and did not include the explicit enzyme environment. An exception is the work of Warshel and co-workers,[25,26] in which the explicit enzyme environment was represented by an electronically adiabatic empirical valence bond (EVB) potential, and nuclear quantum effects were included with path integral methods. This previous work reproduced the magnitude but not the temperature dependence of the experimentally measured KIE. Our vibronically nonadiabatic treatment of this reaction with an EVB potential and a dielectric continuum representation of the enzyme environment resulted in the experimentally observed magnitude and temperature dependence of the rates and KIE.[14] The vibronically nonadiabatic treatment is applicable to systems for which the vibronic coupling, which can be approximated as the product of an electronic coupling and the overlap between the reactant and product hydrogen vibrational wavefunctions, is less than the thermal energy. Our previous calculations indicated that the SLO reaction is vibronically nonadiabatic and illustrated that the proton donor−acceptor motion plays a vital role in facilitating the hydrogen tunneling process. On the other hand, this previous study neglected the explicit enzyme environment and all dynamical effects.

In this paper, we examine the dynamical aspects of the SLO reaction with a vibronically nonadiabatic molecular dynamics method including an explicit enzyme environment. In this approach, the vibronically nonadiabatic rate constant is represented by the time integral of the probability flux correlation function, which is expressed in terms of the vibronic coupling, the average energy gap and proton donor−acceptor distance, and the time correlation functions of the energy gap and the proton donor−acceptor distance.[28−30] This method accounts for the dynamical correlation between the proton donor−acceptor motion and the nonadiabatic transitions between the reactant and product vibronic states. Previously this approach was applied to model PCET reactions in solution,[29,30] but it has not yet been applied to PCET in an enzyme. Here we test the underlying assumptions of this formulation for an enzymatic system and study the dynamical behavior of the protein, substrate, and cofactor. We also investigate the physical basis for the experimentally observed magnitude and temperature dependence of the KIEs for this enzyme reaction.

An outline of the paper is as follows. In section II, we describe the theoretical formulation for vibronically nonadiabatic PCET reactions and the methodology used for the molecular dynamics simulations. Section III presents the results, including the validation of linear response theory for this system, the analysis of the time correlation functions for the protein and proton donor−acceptor motions, and the analysis of the magnitude and temperature dependence of the KIEs. In section IV, we summarize the main findings of this study and discuss potential future directions.

II. Theory and Methods

A. Theoretical Formulation. A variety of theoretical approaches have been developed to study PCET reactions.[31−37] In this paper, we apply a vibronically nonadiabatic dynamical formulation for PCET reactions[28] to the SLO reaction. In this formulation, the active electrons and transferring proton are treated quantum mechanically, and the PCET reaction is described in terms of nonadiabatic transitions between pairs of

(14) Hatcher, E.; Soudackov, A. V.; Hammes-Schiffer, S. *J. Am. Chem. Soc.* **2004**, *126*, 5763−5775.
(15) Glickman, M. H.; Wiseman, J. S.; Klinman, J. P. *J. Am. Chem. Soc.* **1994**, *116*, 793−794.
(16) Hwang, C.-C.; Grissom, C. B. *J. Am. Chem. Soc.* **1994**, *116*, 795−796.
(17) Jonsson, T.; Glickman, M. H.; Sun, S.; Klinman, J. P. *J. Am. Chem. Soc.* **1996**, *118*, 10319−10320.
(18) Borowski, T.; Krol, M.; Chruszcz, M.; Broclawik, E. *J. Phys. Chem. B* **2001**, *105*, 12212−12220.
(19) Borowski, T.; Broclawik, E. *J. Phys. Chem. B* **2003**, *107*, 4639−4646.
(20) Tejero, I.; Eriksson, L. A.; Gonzalez-Lafont, A.; Marquet, J.; Lluch, J. M. *J. Phys. Chem. B* **2004**, *108*, 13831−13838.
(21) Kuznetsov, A. M.; Ulstrup, J. *Can. J. Chem.* **1999**, *77*, 1085−1096.
(22) Tresadern, G.; McNamara, J. P.; Mohr, M.; Wang, H.; Burton, N. A.; Hillier, I. H. *Chem. Phys. Lett.* **2002**, *358*, 489−494.
(23) Knapp, M. J.; Klinman, J. P. *Eur. J. Biochem.* **2002**, *269*, 3113−3121.
(24) Mincer, J. S.; Schwartz, S. D. *J. Chem. Phys.* **2004**, *120*, 7755−7760.
(25) Olsson, M. H. M.; Siegbahn, P. E. M.; Warshel, A. *J. Am. Chem. Soc.* **2004**, *126*, 2820−2828.
(26) Olsson, M. H. M.; Siegbahn, P. E. M.; Warshel, A. *J. Biol. Inorg. Chem.* **2004**, *9*, 96−99.
(27) Siebrand, W.; Smedarchina, Z. *J. Phys. Chem. B* **2004**, *108*, 4185−4195.
(28) Soudackov, A.; Hatcher, E.; Hammes-Schiffer, S. *J. Chem. Phys.* **2005,** *122*, 014505.
(29) Hatcher, E.; Soudackov, A.; Hammes-Schiffer, S. *Chem. Phys.* **2005**, *319*, 93−100.
(30) Hatcher, E.; Soudackov, A.; Hammes-Schiffer, S. *J. Phys. Chem. B* **2005**, *109*, 18565−18574.
(31) Cukier, R. I. *J. Phys. Chem.* **1996**, *100*, 15428−15443.
(32) Cukier, R. I.; Nocera, D. G. *Annu. Rev. Phys. Chem.* **1998**, *49*, 337−369.
(33) Cukier, R. I. *Biochim. Biophys. Acta−Bioenergetics* **2004**, *1655*, 37−44.
(34) Soudackov, A.; Hammes-Schiffer, S. *J. Chem. Phys.* **2000**, *113*, 2385−2396.
(35) Hammes-Schiffer, S. *Acc. Chem. Res.* **2001**, *34*, 273−281.
(36) Georgievskii, Y.; Stuchebrukhov, A. A. *J. Chem. Phys.* **2000**, *113*, 10438−10450.
(37) Mayer, J. M. *Annu. Rev. Phys. Chem.* **2004**, *55*, 363−390.

reactant and product mixed electron−proton vibronic states. The nonadiabatic rate constant is expressed as the time integral of the probability flux correlation function:

$$k = \sum_{\mu} P_{\mu} \sum_{\nu} \frac{1}{\hbar^2} \int_{-\infty}^{\infty} j_{\mu\nu}(t)\, \mathrm{d}t \tag{1}$$

where the summations are over the reactant and product vibronic states, P_μ is the Boltzmann probability for the reactant state μ, and $j_{\mu\nu}(t)$ is the probability flux correlation function for the reactant/product pair of vibronic states $\mu\nu$.

The nonadiabatic coupling $V_{\mu\nu}$ between the reactant and product vibronic states is strongly influenced by the proton donor−acceptor distance R. This coupling can often be approximated as

$$V_{\mu\nu}(R) \approx V^{\mathrm{el}} S_{\mu\nu}(R) \tag{2}$$

where V^{el} is a constant effective electronic coupling and $S_{\mu\nu}(R)$ is the overlap between the reactant and product proton vibrational wavefunctions at distance R. In the region about the equilibrium value of the R-coordinate, this coupling can be approximated to be of the form[29]

$$V_{\mu\nu}(R) \approx V^{\mathrm{el}} S^{(0)}_{\mu\nu} \exp[-\alpha_{\mu\nu}(R - \bar{R}_{\mu})] \tag{3}$$

where $\bar{R}_\mu$ is the equilibrium value of the R-coordinate on the reactant surface μ and $S^{(0)}_{\mu\nu} = S_{\mu\nu}(\bar{R}_\mu)$. Note that the nonadiabatic coupling reflects the quantum mechanical behavior of the transferring proton.

We derived an expression for the probability flux correlation function using linear response theory in conjunction with the form of the coupling given in eq 3.[28] In this case, the probability flux correlation function is expressed as

$$j_{\mu\nu}(t) = |V^{\mathrm{el}} S^{(0)}_{\mu\nu}|^2 \exp\left[\frac{i}{\hbar}\langle \varepsilon_{\mu\nu}\rangle t\right] \exp\{\alpha^2_{\mu\nu}[C_R(0) + C_R(t)]\} \times \exp\left\{-\frac{1}{\hbar^2}\int_0^t \mathrm{d}\tau_1 \int_0^{\tau_1} \mathrm{d}\tau_2 C_{\varepsilon}(\tau_1 - \tau_2)\right\} \tag{4}$$

where $\varepsilon_{\mu\nu}$ is the energy gap (i.e., the difference between the energies of the reactant state μ and the product state ν) for $R = \bar{R}_\mu$, the time correlation functions are defined as

$$C_{\varepsilon}(t) = \langle \delta\varepsilon_{\mu\nu}(0)\, \delta\varepsilon_{\mu\nu}(t)\rangle$$

$$C_R(t) = \langle \delta R(0)\, \delta R(t)\rangle \tag{5}$$

where $\delta\varepsilon_{\mu\nu}(t) = \varepsilon_{\mu\nu}(t) - \langle\varepsilon_{\mu\nu}\rangle$ and $\delta R(t) = R(t) - \langle R\rangle$, and the angular brackets indicate averaging on the reactant vibronic surface. Here we have omitted terms involving the derivative of the energy gap with respect to R because these terms have been shown to be negligible. This formulation of the rate expression is similar to that previously derived for vibrationally nonadiabatic proton transfer reactions occurring on a single adiabatic electronic surface.[38−42]

The input quantities for the probability flux correlation function given in eq 4 can be calculated with classical molecular dynamics simulations of the system on the reactant vibronic surface. The time correlation function $C_R(t)$ and the average value $\bar{R}$ are calculated from classical molecular dynamics simulations on the reactant vibronic surface with an unconstrained R-coordinate. The average energy gap $\langle\varepsilon_{\mu\nu}\rangle$ and the time correlation function $C_\varepsilon(t)$ are calculated from classical molecular dynamics simulations on the reactant vibronic surface with the R-coordinate constrained to $R = \bar{R}$. The energy gap is calculated for each time step using a two-state EVB model representing the reactant and product vibronic surfaces.

To investigate the temperature dependence of the KIEs, we invoke two additional approximations that have been shown to be valid for the SLO reaction. The first approximation relies on the observation that only the initial value of the energy gap correlation function impacts the rate, so the solvent damping term becomes a Gaussian:

$$F_{\varepsilon}(t) \equiv \exp\left\{-\frac{1}{\hbar^2}\int_0^t \mathrm{d}\tau_1 \int_0^{\tau_1} \mathrm{d}\tau_2 C_{\varepsilon}(\tau_1 - \tau_2)\right\} \approx \exp\left\{-\frac{\langle\delta\varepsilon^2\rangle t^2}{2\hbar^2}\right\} \tag{6}$$

In linear response theory, the reorganization energy λ can be expressed in terms of the variance $\langle\delta\varepsilon^2\rangle$ as

$$\lambda = \frac{\langle\delta\varepsilon^2\rangle}{2k_{\mathrm{B}}T} \tag{7}$$

where k_{B} is the Boltzmann constant. The second approximation relies on the representation of $C_R(t)$ by the standard analytical expression for an undamped classical mechanical harmonic oscillator:

$$C_R(t) = \frac{k_{\mathrm{B}}T}{M\Omega^2}\cos\Omega t \tag{8}$$

where Ω is the harmonic oscillator frequency and M is the mass. We have also derived the analogous equations based on the representation of $C_R(t)$ by the standard analytical expression for an undamped quantum mechanical harmonic oscillator. The equations and results are provided in Supporting Information and are qualitatively similar to the results obtained using eq 8.

The overall rate constant can be calculated by numerically integrating the time integral of the probability flux correlation function using the approximations in eqs 6 and 8. Alternatively, to avoid the numerical integration, we can expand the expression in eq 8 in a Taylor series to second order in time and analytically integrate the time integral of the resulting probability flux correlation function. This procedure leads to the rate expression

$$k = \sum_{\mu} P_{\mu} \sum_{\nu} \frac{|V^{\mathrm{el}} S^{(0)}_{\mu\nu}|^2}{\hbar} \exp\left[\frac{2k_{\mathrm{B}}T\alpha^2_{\mu\nu}}{M\Omega^2}\right] \sqrt{\frac{\pi}{(\lambda + \lambda_{\alpha})k_{\mathrm{B}}T}} \times \exp\left[-\frac{(\Delta G^{\circ} + \lambda + \Delta\epsilon_{\mu\nu})^2}{4(\lambda + \lambda_{\alpha})k_{\mathrm{B}}T}\right] \tag{9}$$

where $\lambda_\alpha = \hbar^2\alpha^2_{\mu\nu}/2M$, ΔG° is the driving force, and $\Delta\epsilon_{\mu\nu}$ is the difference between the product and reactant vibronic energy

(38) Borgis, D.; Lee, S.; Hynes, J. T. *Chem. Phys. Lett.* **1989**, *162*, 19−26.
(39) Borgis, D.; Hynes, J. T. *J. Chem. Phys.* **1991**, *94*, 3619−3628.
(40) Suarez, A.; Silbey, R. *J. Chem. Phys.* **1991**, *94*, 4809−4816.
(41) Trakhtenberg, L. I.; Klochikhin, V. L.; Pshezhetsky, S. Y. *Chem. Phys.* **1982**, *69*, 121−134.
(42) Kiefer, P. M.; Hynes, J. T. *Solid State Ionics* **2004**, *168*, 219.

levels relative to the ground states. Here we have used the linear response relation $\langle\varepsilon\rangle = \Delta G^\circ + \lambda$ and the expression for the reorganization energy in eq 7. The derivation of eq 9 also assumes that the time correlation functions for the R-coordinate and the energy gap (i.e., the reorganization energy) are the same for all vibronic states. This rate expression is similar to the Marcus theory expression for electron transfer except for the factor of $\exp[2k_BT\alpha_{\mu\nu}^2/M\Omega^2]$, the term λ_α in the two denominators, and the inclusion of the overlap factor in the vibronic coupling.

If we make one additional approximation, we can obtain a remarkably simple, approximate expression for the KIE, which is the ratio of the rate constants for hydrogen transfer and deuterium transfer. As will be shown below, the R-coordinate term in eq 4 is approximately constant on the time scale of the probability flux correlation function decay for the SLO reaction, so we can invoke the approximation that $C_R(t) \approx C_R(0)$. In this case, the R-coordinate term in eq 4 can be simplified to be

$$F_R(t) \equiv \exp\{\alpha_{\mu\nu}^2[C_R(0) + C_R(t)]\} \approx \exp\{2\alpha_{\mu\nu}^2 C_R(0)\} \quad (10)$$

Using the approximations in eqs 6, 8, and 10, the time integral of the probability flux can be integrated analytically to give the rate expression

$$k = \sum_\mu P_\mu \sum_\nu \frac{|V^{el}S_{\mu\nu}^{(0)}|^2}{\hbar} \exp\left[\frac{2k_BT\alpha_{\mu\nu}^2}{M\Omega^2}\right]\sqrt{\frac{\pi}{\lambda k_BT}} \times \exp\left[-\frac{(\Delta G^\circ + \lambda + \Delta\epsilon_{\mu\nu})^2}{4\lambda k_BT}\right] \quad (11)$$

This rate expression is similar to the Marcus theory expression for electron transfer except for the factor of $\exp[2k_BT\alpha_{\mu\nu}^2/M\Omega^2]$ and the inclusion of the overlap factor in the vibronic coupling. It differs from eq 9 by the absence of the term λ_α in the two denominators.

The rate expression in eq 11 leads to a relatively simple expression for the KIE because only the first two factors depend on the isotope. If we consider only the nonadiabatic transition between the two ground states, the KIE can be approximated as

$$\mathrm{KIE} \approx \frac{|S_H|^2}{|S_D|^2}\exp\left\{\frac{2k_BT}{M\Omega^2}(\alpha_H^2 - \alpha_D^2)\right\} \quad (12)$$

where S_H and S_D are the overlaps of the hydrogen and deuterium wavefunctions, respectively, and α_H and α_D represent the exponential dependence of this overlap on R for hydrogen and deuterium, respectively. Note that the quantity $k_BT/M\Omega^2 = C_R(0) = \langle\delta R^2\rangle$ and can be calculated directly from the molecular dynamics simulations. Similarly, the reorganization energy λ given by eq 7 and the quantity $\Delta G^\circ + \lambda = -\langle\varepsilon\rangle$ can also be calculated directly from the molecular dynamics simulations. The simplified expression for the KIE given in eq 12 provides insight into the magnitude and temperature dependence of the KIE for the lipoxygenase system. The effects of excited vibronic states can be included by summing over these states in eq 11.

In order to calculate the rates and KIEs, the overlaps of hydrogen and deuterium wavefunctions, S_H and S_D, and the vibronic coupling parameters, α_H and α_D, must be calculated. These quantities can be estimated from one-dimensional nuclear wavefunctions for Morse potentials corresponding to C−H and O−H vibrational modes. The standard expression for the Morse potential is given by

$$E_{XY} = D_{XY}(e^{-2\beta_{XY}(R_{XY}-R_{XY}^\circ)} - 2e^{-\beta_{XY}(R_{XY}-R_{XY}^\circ)}) \quad (13)$$

The values for D_{CH} and D_{OH} were determined to be 77 and 82 kcal/mol, respectively, on the basis of the bond dissociation energies.[9,43,44] The values for β_{CH} and β_{OH} were determined to be 2.068 and 2.442 Å^{-1}, respectively, to reproduce the typical experimentally measured C−H and O−H frequencies of 2900 and 3500 cm^{-1}.[45] The values for R_{CH}^o and R_{OH}^o were determined to be 1.09 and 0.96 Å, respectively, from the experimentally measured bond lengths.[45] All of these values are similar to the values used in our previous study.[14] The hydrogen and deuterium vibrational wavefunctions for the Morse potentials are calculated analytically.[46] The overlaps between the reactant and product wavefunctions are calculated numerically, and the α_H and α_D parameters are calculated with the finite difference method using the relation $\alpha = d\ln S/dR$ for the equilibrium value $\bar{R}$. The values of the overlaps and the α_H and α_D parameters can be calculated in this manner for both ground and excited vibrational states. For $\bar{R} = 2.87$ Å, we found that $\alpha_H = 22.74$ Å^{-1}, $\alpha_D = 32.84$ Å^{-1}, $S_H = 3.87 \times 10^{-5}$, and $S_D = 3.37 \times 10^{-7}$ for the ground states.

We investigated the sensitivity of the magnitude and temperature dependence of the KIE on the Morse potential parameters and the equilibrium value $\bar{R}$. In general, we found that the results did not change qualitatively when the Morse potential parameters were varied within physically reasonable ranges. The equilibrium value $\bar{R}$ strongly impacts the overlaps S_H and S_D but only weakly influences the α_H and α_D parameters within a physically reasonable range of the R-coordinate. Based on eq 12, this analysis indicates that the temperature dependence of the KIE is not significantly influenced by $\bar{R}$, but the magnitude of the KIE is strongly impacted by $\bar{R}$. These trends are quantified by a table provided in the Supporting Information. For the calculations in this paper, the equilibrium value $\bar{R}$ was not a free parameter but rather was obtained directly from the molecular dynamics simulations.

A PCET reaction is vibronically nonadiabatic when the vibronic coupling is significantly less than the thermal energy k_BT. In this reaction, the electron is transferring from the π system of the substrate to the iron of the cofactor. On the basis of the approximate expression for the vibronic coupling in eq 2 and the calculated value of $\sim 10^{-5}$ for the overlap, the electronic coupling is expected to be well below the value required for vibronic nonadiabaticity at room temperature. Thus, our calculations indicate that this PCET reaction is vibronically nonadiabatic.

B. Molecular Dynamics Simulations. We used an X-ray crystallographic structure of soybean lipoxygenase-1 (PDB code 1YGE)[10] for the initial coordinates in our simulations. The linoleic acid substrate was inserted into the substrate cavity of the crystal structure using the AutoDock 3.0.5 docking pro-

(43) Mayer, J. M. *Acc. Chem. Res.* **1998**, *31*, 441−450.
(44) Clark, K. B.; Culshaw, P. N.; Griller, D.; Lossing, F. P.; Simoes, J. A. M.; Walton, J. C. *J. Org. Chem.* **1991**, *56*, 5535−5539.
(45) Warshel, A. *Computer Modeling of Chemical Reactions in Enzymes and Solutions*; John Wiley & Sons, Inc.: New York, 1991.
(46) Dahl, J. P.; Springborg, M. *J. Chem. Phys.* **1987**, *88*, 4535.

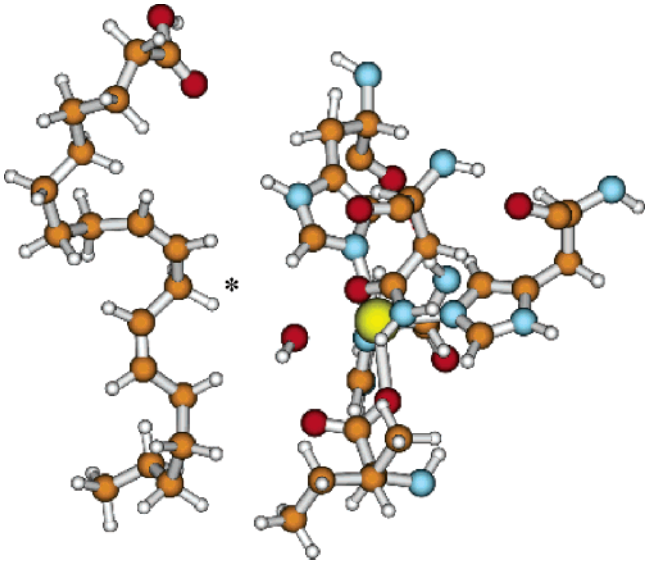

Figure 2. Iron cofactor (right) and lipoxygenase and the substrate linoleic acid (left). The transferring hydrogen is identified with an asterisk.

gram.[47] The initial conformation of the linoleic acid was chosen on the basis of the lowest energy conformation of 250 different conformations. The starting conformations of the iron cofactor and linoleic acid substrate are depicted in Figure 2. The protonation states of the residues within the protein were calculated according to the Poisson−Boltzmann method using the H++ database.[48,49] Subsequently, we replaced a peripheral water with a sodium cation to neutralize the overall charge of the system. The protein and substrate were centered in a truncated octahedral periodic box with dimensions 139 Å × 139 Å × 139 Å and were solvated with 12 772 explicit TIP3P[50−52] water molecules.

The potential energy surface used for the molecular dynamics simulations is based on the AMBER99 force field.[52] We used the RESP method[53] to determine the partial charges of the neutral (reactant) and the radical (product) forms of linoleic acid. For this purpose, the structure of linoleic acid was optimized using density functional theory at the B3LYP/6-31G** level, and the partial atomic charges were calculated for the reactant and product forms at the MP2/6-31G* level. All of these electronic structure calculations were performed with Gaussian03.[54] The Fe−ligand bonds and ligand−Fe−ligand angles in the iron cofactor were represented by harmonic potentials. For the Fe−ligand bonds, the equilibrium distances were set to the distances optimized previously with DFT calculations,[14] and the force constants were obtained from experimental studies of model iron systems.[55] For the ligand−Fe−ligand angles, the equilibrium angles were set to the octahedral positions of 90° and 180°, and the force constants were set to 125 kcal/mol·rad^2. The Fe−O−H angle for the hydroxyl ligand was represented by a harmonic potential with the equilibrium angle of 126° and a force constant of 100 kcal/mol·rad^2, similar to the parameters used previously for a Zn−O−H angle.[56] The Fe−O−C angle for the Ile839 ligand was represented by a harmonic potential with an equilibrium angle of 128° and a force constant of 70 kcal/mol·rad^2, similar to the values used previously for an iron transferrin system.[57]

The simulations were performed with a modified version of DLPROTEIN[58,59] that includes the EVB method. A two-state EVB model for the system was used to calculate the energy gap between the reactant and product states. The transferring electron and proton are localized on the linoleic acid substrate in the reactant and on the iron cofactor in the product. A two-state EVB model is applicable for this system because the intermediate diabatic PCET states, in which only the electron or only the proton has transferred, are much higher in energy than the reactant and product states. The modified AMBER force field is used to describe both EVB states. To account for the difference in the zero of energy for the two potential energy surfaces, a constant energy shift Δ is added to the product state potential. As described below, the value of Δ is determined by linear response theory relations.

We emphasize that this solvated enzyme system includes ~52 000 atoms and that all of these atoms are moving in our molecular dynamics simulations. In other words, we are not freezing any part of the system. The Ewald method[60] was used to treat long-range electrostatic interactions. The classical equations of motion were integrated with the velocity Verlet algorithm[61] on the reactant vibronic surface with a time step of 1 fs. All bond lengths involving hydrogen atoms were constrained with the SHAKE algorithm.[62] Both the NPT and the NVT simulations were performed with Nosé−Hoover thermostats.[63,64]

The system was carefully equilibrated prior to data collection. To avoid dissociation of the linoleic acid substrate, the distance between the C11 carbon of the linoleic acid and the oxygen atom of the hydroxyl ligand of the iron cofactor was constrained to 3.2 Å, which is approximately the sum of the van der Waals radii of carbon and oxygen, during the equilibration procedure. In the first step of equilibration, a minimization of the entire system was performed. In the second step, molecular dynamics simulations were propagated for 50 ps at 100, 200, and 300 K with an NPT ensemble. The NPT ensemble was used to relax the volume of the box and to avoid vacuum bubbles in the solvent. In the third step of the equilibration procedure, the molecular dynamics simulations were propagated for 100 ps with an NVT ensemble at 300 K. The root-mean-square deviation of the backbone of the protein after equilibration was calculated to be 1.48 Å.[65]

(47) Morris, G. M.; Goodsell, D. S.; Halliday, R. S.; Huey, R.; Hart, W. E.; Belew, R. K.; Olson, A. J. *J. Comput. Chem.* **1998**, *19*, 1639−1662.
(48) Bashford, D.; Karplus, M. *Biochemistry* **1990**, *29*, 10219−10225.
(49) Gordon, J. C.; Myers, J. B.; Folta, T.; Shoja, V.; Heath, L. S.; Onufriev, A. *Nucleic Acids Res.* **2005**, *33*, W368−W371.
(50) Jorgensen, W. L. *J. Am. Chem. Soc.* **1981**, *103*, 335.
(51) Jorgensen, W. L.; Chandreskhar, J.; Madura, J. D.; Impey, R. W.; Klein, M. L. *J. Chem. Phys.* **1982**, *79*, 926−935.
(52) Cornell, W. D.; Cieplak, P.; Bayly, C. I.; Gould, I. R.; Merz, K. M., Jr.; Ferguson, D. M.; Spellmeyer, D. C.; Fox, T.; Caldwell, J. W.; Kollman, P. A. *J. Am. Chem. Soc.* **1995**, *117*, 5179−5197.
(53) Bayly, C.; Cieplak, P.; Cornell, W.; Kollman, P. A. *J. Phys. Chem.* **1993**, *97*, 10269−10280.
(54) Frisch, M. J.; et al. *Gaussian 03*, revision C.03; Gaussian, Inc.: Pittsburgh, PA, 2003.
(55) Zhou, Z.; Khan, S. U. M. *J. Phys. Chem.* **1989**, *93*, 5292−5295.
(56) Hoops, S. C.; Anderson, K. W.; Merz, K. M. *J. Am. Chem. Soc.* **1991**, *113*, 8262−8270.
(57) Lin, W.; Welsh, W. J.; Harris, W. R. *Inorg. Chem.* **1994**, *33*, 884−890.
(58) Melchionna, S.; Cozzini, S. *DLPROTEIN*, 2.1; Rome, Italy, 2001.
(59) Smith, W.; Forester, T. R. *DL_POLY_2.14*, CCLRC: Daresbury Laboratory, Warrington, England, 2003.
(60) Ewald, P. P. *Ann. Phys.* **1921**, *64*, 253−287.
(61) Verlet, L. *Phys. Rev.* **1967**, *159*, 98−103.
(62) Ryckaert, J. P.; Ciccotti, G.; Berendsen, H. J. C. *J. Comput. Phys.* **1977**, *23*, 327.
(63) Hoover, W. G. *Phys. Rev. A* **1985**, *31*, 1695−1697.
(64) Nosé, S. *Mol. Phys.* **1984**, *52*, 255−268.

A final preparation step was performed after this equilibration procedure. For this step and the data collection, the constraint between the C11 carbon of the linoleic acid and the oxygen from the hydroxyl ligand was released, and a weak harmonic angle restraint was applied to the corresponding C−H−O angle to ensure sampling of the region of phase space relevant to hydrogen abstraction. This angle restraint was represented by an equilibrium angle of 180° and a force constant of 10 kcal/mol·rad^2. The final preparation step was required because we found that the substrate dissociated during the data collection procedure, which requires at least 100 ps of sampling. Therefore, an initial molecular dynamics simulation was propagated for 50 ps at 303 K to provide an estimate of the average distance between the C11 carbon of the linoleic acid and the iron of the cofactor. This distance was subsequently constrained to its average value of 4.4 Å to avoid dissociation of the substrate but still enable the sampling of the proton donor−acceptor distance through vibrational motions of the oxygen and librational motions of the entire substrate and cofactor. This procedure could be viewed as providing an associated reactive complex that would be formed on a much slower time scale than can be sampled with computer simulations.

The first stage of data collection involved molecular dynamics simulations on the reactant vibronic surface with an unconstrained R-coordinate (i.e., without a constraint between the C11 carbon of the linoleic acid and the oxygen of the hydroxyl group of the iron cofactor). We sampled the entire system for 100 ps at 303 K. The average proton donor−acceptor distance was determined to be $\bar{R} = 2.87$ Å. We also calculated the variance of the proton donor−acceptor mode coordinate to be $C_R(0) = \langle \delta R^2 \rangle = 0.00406$ Å^2. Using eq 8, the quantity $M\Omega^2$ was determined directly from this variance, and the effective frequency Ω was determined from the time dependence of the R-coordinate term $F_R(t)$ on the time scale of the probability flux correlation function decay. Note that the effective mass and frequency of the proton donor−acceptor mode are determined directly and uniquely from the molecular dynamics simulations, thereby avoiding the arbitrary choice of mass and frequency. We tested for convergence by calculating the basic quantities for two halves of the molecular dynamics data and found that the average proton donor−acceptor distance differed by less than 0.01 Å and the variance differed by 0.0003 Å^2 for the two portions of the data.

The second stage of data collection involved molecular dynamics simulations on the reactant vibronic surface with the proton donor−acceptor distance constrained to the average distance determined in the first stage. We sampled the system for 50 ps at 303 K during this stage. We calculated the average energy gap $\langle \varepsilon_{\mu\nu} \rangle$ and the time correlation function of the energy gap $C_\varepsilon(t)$ to use as input into the rate expression given above. The energy gap between the reactant and product vibronic states was calculated with a two-state EVB model. At each time step, the product energy was calculated by moving the transferring hydrogen, H*, to the acceptor oxygen in the Fe−O−H plane, with an O−H* distance of 0.9572 Å and an H*−O−H angle of 104.5°. The energy gap $\varepsilon_{\mu\nu}$ was calculated as the difference between the energies of the reactant and product states, excluding the bonding interactions directly involving the transferring hydrogen because this hydrogen nucleus behaves quantum mechanically. We tested for convergence by comparing the results for two halves of the 50 ps molecular dynamics simulation and found that the average energy gap differed by only ∼2%. We also compared the results for two independent 25 ps molecular dynamics simulations and found that the average energy gap differed by only ∼5% for these two independent simulations.

Our analysis indicates that the duration of these simulations is sufficient for studying the PCET reaction. Since the time correlation functions of the energy gap and the R-coordinate decay in less than 1 ps, and the probability flux correlation function decays in less than 10 fs, these simulations should capture the motions on the relevant time scale for the PCET reaction. As mentioned above, we also tested the convergence by comparing the results from separate portions of the data and independent trajectories. On the other hand, these simulations are short relative to larger conformational changes of the protein. Such conformational changes of the protein may be involved in the formation of the associated reactive complex. The protein was crystallized in the absence of the linoleic substrate, and we determined the initial substrate configuration from docking simulations followed by equilibration of the entire system. In general, these types of simulations may not capture the slower conformational changes induced by substrate binding.

The overall rate constant is obtained by summing over the contributions from all pairs of reactant and product vibronic states. The probability flux correlation function can be determined for any pair of reactant and product vibronic states by calculating the overlaps and α_H and α_D parameters for the corresponding vibrational states of the Morse potentials, as well as the relevant vibrational energy level splittings $\Delta\epsilon_{\mu\nu}$. This procedure is based on the approximation that the time correlation functions for the R-coordinate and the energy gap (i.e., the reorganization energy) do not change significantly for the different vibronic states. For the SLO reaction, we found that the rates and KIEs are converged by including contributions from the ground and first excited vibronic states for the reactant and the product.

III. Results and Discussion

A. Validation of Linear Response Theory. We test the validity of the linear response approximation for this system by analyzing the energy gap calculations obtained from the molecular dynamics simulations. The energy gap distribution function $P(\varepsilon)$ is calculated by binning the energy gap values over 100 bins in the range from −20 to −70 kcal/mol. The energy gap distribution function $P(\varepsilon)$, which is shown in Figure 3a, resembles a Gaussian distribution with the center at $\varepsilon = \langle \varepsilon \rangle$ and the width determined by the variance of the energy gap, $\langle \delta\varepsilon^2 \rangle$. The free energy calculated from the energy gap distribution function is depicted in Figure 3b. In the linear response regime, the free energy curve is a parabola with minimum $\langle \varepsilon \rangle$ and force constant $f_{harm} = k_B T/\langle \delta\varepsilon^2 \rangle$. The corresponding harmonic free energy curve from linear response theory is also depicted in Figure 3b. The agreement between this harmonic free energy curve and the free energy curve calculated from the molecular dynamics simulations provides validation for the linear response approximation for this system. Note that a complete validation of the linear response approximation

(65) Humphrey, W.; Dalke, A.; Schulten, K. *J. Mol. Graphics* **1996**, *14*, 33−38.

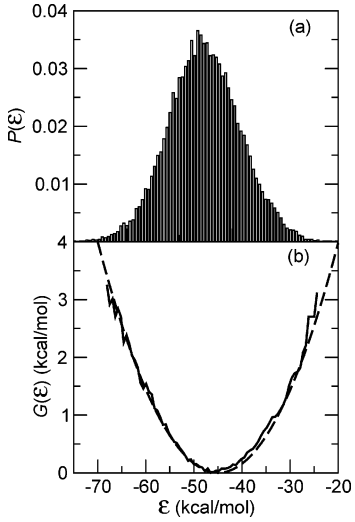

Figure 3. (a) Energy gap distribution function $P(\varepsilon)$ and (b) the free energy curve calculated from this distribution function using $G(\varepsilon) = -k_B T \ln[P(\varepsilon)]$ (solid) and from the linear response approximation of a parabola with minimum $\langle\varepsilon\rangle$ and force constant $f_{harm} = k_B T/\langle\delta\varepsilon^2\rangle$ (dashed).

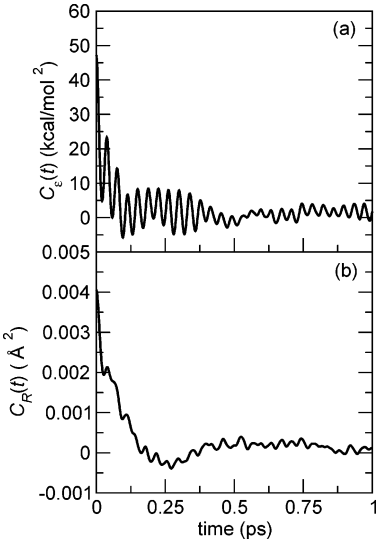

Figure 4. Time correlation functions of (a) the energy gap and (b) the *R*-coordinate.

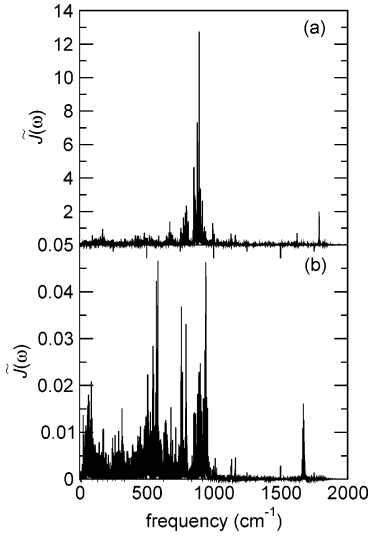

Figure 5. Normalized spectral density corresponding to (a) $C_\varepsilon(t)$ and (b) $C_R(t)$. The normalized spectral density is defined as $\tilde{J}(\omega) = J(\omega)/\int_0^\infty J(\omega)/\omega\, d\omega$, where the spectral density $J(\omega)$ is calculated from the time correlation function using the relation $C(t) = 8/\pi\beta \int_0^\infty J(\omega)/\omega \cos(\omega t)\, d\omega$.

requires the product free energy curve to be harmonic with the same frequency. Since the product state is defined to be a local perturbation of the reactant state, this criterion is expected to be satisfied as well.

Within the framework of linear response theory, the reorganization energy can be expressed in terms of the variance $\langle\delta\varepsilon^2\rangle$ according to eq 7, and the average energy gap can be related to the driving force $\Delta G°$ and the reorganization energy λ as $\langle\varepsilon\rangle = -(\Delta G° + \lambda)$. Since we have illustrated the validity of linear response theory for this system, we can use these relations to determine the constant energy shift Δ between the reactant and product state potential energy surfaces. The free energy of reaction, $\Delta G°$, was estimated to be -5.4 kcal/mol for the SLO system on the basis of experimental data.[14] The average energy gap and the variance of the energy gap were calculated from the molecular dynamics simulations to be $\langle\varepsilon\rangle = -\Delta - 44.96$ kcal/mol and $\langle\delta\varepsilon^2\rangle = 47.17$ (kcal/mol)^2, respectively. Using the linear response theory relations given above, we determine that $\Delta = -11$ kcal/mol. The reorganization energy is calculated from the molecular dynamics simulations to be $\lambda = 39$ kcal/mol. Our analysis indicates that ~18 kcal/mol of this total reorganization energy is due to reorganization of the iron cofactor.

B. Time Correlation Functions for Protein and Proton Donor−Acceptor Motions. The time correlation functions $C_\varepsilon(t)$ and $C_R(t)$ for the energy gap and *R*-coordinate, respectively, are calculated from the molecular dynamics simulations described above. These time correlation functions are depicted in Figure 4. Both time correlation functions decay quickly within 0.5 ps. The normalized spectral densities corresponding to $C_\varepsilon(t)$ and $C_R(t)$, respectively, are shown in Figure 5. Figure 5a depicts the spectral density of the energy gap correlation function, which corresponds to the vibrations within the protein. Figure 5b depicts the spectral density corresponding to the proton donor−acceptor motion.

The probability flux correlation function is calculated from eq 4 with the time correlation functions obtained from the molecular dynamics simulations. The normalized real part of the probability flux correlation function is depicted in Figure 6a. The ground state rate constant is calculated by integrating this probability flux correlation function over time. As illustrated in Figure 6a, the probability flux correlation function decays quickly, in ~10 fs. The probability flux correlation function can be decomposed into the quantum coherent term, the solvent damping term, and the *R*-coordinate term. These components are depicted in Figure 6b.

An analysis of the components comprising the probability flux correlation function provides insight into the roles of the protein and the proton donor−acceptor motions. The quantum coherent term, $F_Q(t)$, is a highly oscillatory function with a period determined by the average energy gap, $\langle\varepsilon\rangle$. As indicated by eq 6, the protein/solvent damping term, $F_\varepsilon(t)$, decays on a time scale determined by the energy gap variance $\langle\delta\varepsilon^2\rangle$, which is directly related to the reorganization energy through eq 7. Since the protein/solvent damping term decays on a much faster time scale than the other components of the probability flux correlation function, this term dictates the decay time of the

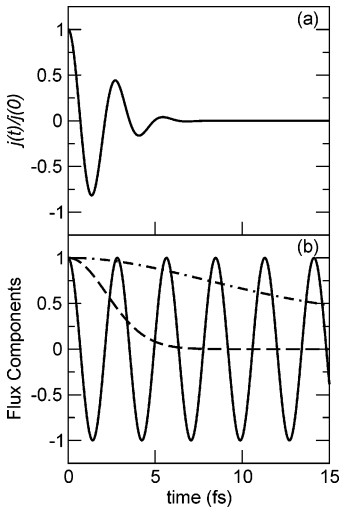

Figure 6. (a) Time dependence of the real part of the normalized probability flux correlation function given in eq 4 and (b) time dependence of the normalized probability flux components calculated from molecular dynamics simulations at 303 K. The components include the quantum coherent term, $F_Q(t) = \exp[i\langle\varepsilon\rangle t/\hbar]$ (solid), the solvent damping term $F_\varepsilon(t)$ defined in eq 6 (dashed), and the R-coordinate term $F_R(t)$ defined in eq 10 (dot-dashed).

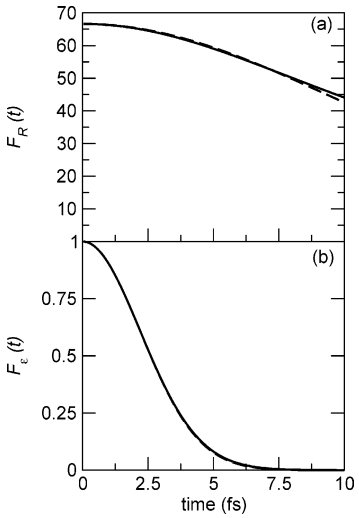

Figure 7. (a) Comparison of the R-coordinate term $F_R(t)$ calculated with $C_R(t)$ from the classical molecular dynamics simulations (solid) to this term calculated with $C_R(t)$ for an undamped classical harmonic oscillator given in eq 8 (dashed). (b) Comparison of the solvent damping term $F_\varepsilon(t)$ calculated with $C_\varepsilon(t)$ from the classical molecular dynamics simulations (solid) to this term calculated with the short-time approximation given in eq 6 (dashed). Note that the solid and dashed curves are virtually indistinguishable.

probability flux correlation function. As indicated by eq 7, a larger reorganization energy leads to a faster decay of the probability flux correlation function and therefore a slower overall rate. Figure 6b illustrates that the R-coordinate term, $F_R(t)$, is relatively constant on the time scale of the decay of the probability flux correlation function. This observation indicates that the dynamical behavior of the R-coordinate [i.e., the time dependence of $C_R(t)$] does not significantly impact the time dependence of the probability flux correlation function. The magnitude of $F_R(t)$, however, greatly impacts the magnitude of the probability flux correlation function and therefore the magnitude of the overall rate. As indicated by the definition of $F_R(t)$ in eq 10, the magnitude of the overall rate is strongly influenced by the variance of the R-coordinate, $C_R(0) = \langle\delta R^2\rangle$, which is related to the frequency of the proton donor−acceptor motion as in eq 8, and the parameter α, which represents the dependence of the vibronic coupling on the R-coordinate as in eq 3.

We also test two additional approximations invoked to study the temperature dependence of the rates and the KIEs. The first approximation is the short-time approximation, in which only equilibrium fluctuations of the solvent and protein are considered. This approximation is valid when the decay time of the probability flux correlation function is short with respect to the initial decay time of the energy gap correlation function. In this limit, only the initial value of the energy gap correlation function impacts the rate, leading to the simplified protein/solvent damping term given in eq 6. In the second approximation, the R-coordinate time correlation function is represented by the time correlation function of an undamped, classical harmonic oscillator, as given in eq 8. Thus, the R-coordinate motion is represented by an effective harmonic mode, and the damping effects on this mode from the solvent and protein environment are assumed to be negligible on the time scale of the decay of the probability flux correlation function. The quantity $M\Omega^2$ is determined directly from the variance, $k_BT/M\Omega^2 = \langle\delta R^2\rangle = 0.00406$ Å^{-2}, and the effective frequency is determined from the time dependence of the R-coordinate term $F_R(t)$ on the time scale of the probability flux correlation function decay. The resulting effective mass and frequency are $M = 14$ amu and $\Omega = 353$ cm^{-1}. These values suggest that the local component of the proton donor−acceptor mode is dominant. As shown by Figure 5b, however, this effective mode reflects a variety of vibrational motions. Figure 7 illustrates that these approximations for the energy gap and R-coordinate correlation functions are reasonable for the PCET reaction catalyzed by SLO.

C. Temperature Dependence of KIEs. We calculate the magnitude and temperature dependence of the KIE using both the simple approximate expression in eq 12 and the more quantitatively accurate expression in eq 9. The average energy gap and the time correlation functions for the energy gap and the R-coordinate are calculated from the molecular dynamics simulations at 303 K. The overlaps S_H and S_D and the parameters α_H and α_D are calculated from the hydrogen and deuterium vibrational wavefunctions corresponding to Morse potentials, with the donor and acceptor atoms separated by the equilibrium value $\bar{R} = 2.87$ Å determined from the molecular dynamics simulations. The Morse potentials and the corresponding ground state hydrogen and deuterium vibrational wavefunctions are depicted in Figure 8. Since the KIE is the ratio of two rates, the KIE is independent of the constant electronic coupling parameter V^{el}, and we do not need to determine the value of this parameter. For these calculations, we do not fit any parameters directly to the experimental kinetic data.

The temperature dependence of the KIE using the simple approximate expression in eq 12 is depicted in Figure 9. The quantity $M\Omega^2$ is determined from the R-coordinate variance, $C_R(0) = k_BT/M\Omega^2 = \langle\delta R^2\rangle$, obtained from the molecular dynamics simulations at 303 K. Equation 12 indicates that the temperature dependence of the KIE is determined mainly by the effective proton donor−acceptor frequency and the parameters α_H and α_D. The ratio of the overlaps of the hydrogen and deuterium vibrational wavefunctions strongly impacts the magnitude of the KIE but does not affect the temperature

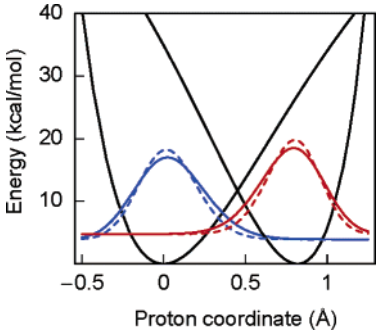

Figure 8. Morse potentials and the corresponding hydrogen (solid) and deuterium (dashed) vibrational wavefunctions for the reactant (blue) and product (red) states. For illustrative purposes, the zero-point energy for deuterium was increased to be the same as the zero-point energy for hydrogen.

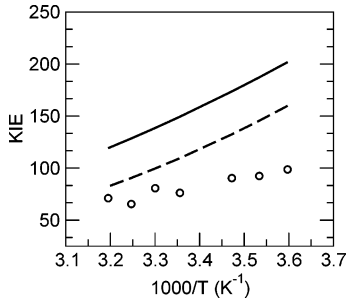

Figure 9. Temperature dependence of the KIE obtained with the simple approximate expression in eq 12 (solid line) and the analogous expression including the excited vibronic states (dashed line). The experimental data are depicted with circles.

dependence. This simple approximate expression leads to qualitative agreement with the experimentally observed temperature dependence of the KIE but overestimates the magnitude of the KIE. As mentioned above, the values of the overlaps S_H and S_D are sensitive to the equilibrium value of the *R*-coordinate, which is obtained directly from the molecular dynamics simulations.

We include the effects of the excited vibronic states using the rate expression in eq 11. For hydrogen, the contribution from the transition between the ground reactant and product states is 96% at 303 K. For deuterium, the contribution from the transition between the ground states is 70%, and the contribution from the transition between the ground reactant state and the first excited product state is 18% at 303 K. The remaining contributions arise from transitions between the first excited reactant state and the lowest two product states. As shown in Figure 9, including the excited states does not significantly alter the temperature dependence of the KIE but decreases the magnitude of the KIE by ~15%.

Figure 10 depicts the temperature dependence of the KIE using the more quantitatively accurate expression in eq 9, as well as the numerical integration of the probability flux correlation function given in eq 4, in conjunction with the approximations given in eqs 6 and 8. Both of these approaches include the time dependence of the *R*-coordinate time correlation function and the contributions of the excited vibronic states. The results from these two approaches are virtually identical and agree well with the experimentally observed magnitude and temperature dependence of the KIE. We emphasize that the magnitude and temperature dependence of the KIE are obtained without fitting any parameters directly to the kinetic data. The

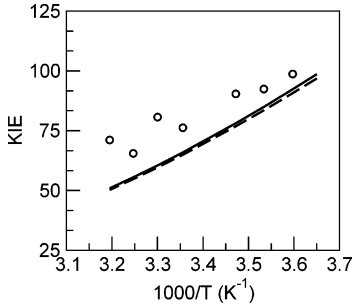

Figure 10. Temperature dependence of the KIE obtained with the rate expression in eq 9 (solid line) and by numerical integration of the probability flux correlation function given in eq 4 in conjunction with the approximations in eqs 6 and 8 (dashed). Both calculations include the contributions of the excited vibronic states. Note that the solid and dashed lines are virtually indistinguishable. The experimental data are depicted with circles.

large magnitude of the KIE arises from the relatively small overlap of the reactant and product hydrogen vibrational wavefunctions, leading to a large value for the ratio of the hydrogen and deuterium overlaps, as well as the dominance of the ground vibronic states. The weak temperature dependence of the KIE arises mainly from the dominance of the local component of the proton donor−acceptor motion. The corresponding calculations with an approximate quantum mechanical treatment of the *R*-coordinate also agree well with the experimental data and are provided in the Supporting Information. This agreement between the theoretical and experimental KIEs suggests that this theoretical formulation contains the essential physical elements for these types of reactions.

IV. Conclusions

In this paper, we examined the dynamical behavior and the temperature dependence of the kinetic isotope effects for the PCET reaction catalyzed by SLO. Our calculations were based on a vibronically nonadiabatic formulation for PCET reactions in solution and proteins. This formulation includes the quantum mechanical effects of the active electrons and the transferring proton, as well as the motions of all atoms in the complete solvated enzyme system. The rate is represented by the time integral of a probability flux correlation function that depends on the vibronic coupling, the average of the energy gap and *R*-coordinate, and the time correlation functions of the energy gap and *R*-coordinate. The vibronic couplings can be estimated to within a constant factor by calculating the overlaps between reactant and product hydrogen vibrational wavefunctions for model systems, and the other quantities can be calculated from classical molecular dynamics simulations of the entire system.

We tested the underlying assumptions of this vibronically nonadiabatic formulation for the SLO enzyme reaction and investigated the dynamical behavior of the protein, substrate, and cofactor. Our estimates of the contributions to the vibronic couplings for this PCET reaction indicate that this reaction is vibronically nonadiabatic. Moreover, our molecular dynamics simulations of the entire solvated enzyme system provide validation for the linear response approximation for this PCET reaction and provide an estimate of 39 kcal/mol for the total reorganization energy. We found that the dynamical behavior (i.e., the time dependence) of the probability flux correlation function is dominated by the equilibrium protein and solvent motions and is not significantly influenced by the proton donor−acceptor motion. The magnitude of the overall rate, however,

is strongly influenced by the frequency of the proton donor−acceptor motion, the magnitude and distance dependence of the vibronic coupling, and the protein/solvent reorganization energy.

These calculations reproduced the experimentally observed magnitude and temperature dependence of the KIE for the SLO enzyme reaction without fitting any parameters directly to the experimental kinetic data. The temperature dependence of the KIEs is determined mainly by the effective proton donor−acceptor frequency, which can be calculated from the *R*-coordinate variance in the molecular dynamics simulations, and the distance dependence of the vibronic couplings for hydrogen and deuterium, which can be calculated from the vibrational wavefunctions for model systems. The ratio of the overlaps of the hydrogen and deuterium vibrational wavefunctions strongly impacts the magnitude of the KIE but does not significantly influence the temperature dependence. These trends are summarized in the relatively simple, approximate expression for the KIE given in eq 12. For the SLO reaction, the large magnitude of the KIE arises mainly from the dominance of tunneling between the ground vibronic states and the relatively large ratio of the overlaps between the corresponding hydrogen and deuterium vibrational wavefunctions. The weak temperature dependence of the KIE is due in part to the dominance of the local component of the proton donor−acceptor motion.

These calculations provide insight into the fundamental physical principles underlying the PCET reaction catalyzed by SLO. Future studies will focus on the impact of mutations on the dynamical behavior of the protein, substrate, and cofactor and on the magnitude and temperature dependence of the KIEs for this reaction. This general theoretical formulation is applicable to a broad range of other vibronically nonadiabatic enzyme reactions.

Acknowledgment. We are grateful for support of this work by NIH grant GM56207 and NSF grant CHE-05-01260.

Supporting Information Available: Force field parameters used for the iron cofactor; data used to create Figures 9 and 10; sensitivity analysis for the dependence of the vibronic coupling contributions to the kinetic isotope effect on the equilibrium proton donor−acceptor distance; temperature dependence of the KIEs from calculations including the quantum mechanical effects of the *R*-coordinate; and complete ref 54. This material is available free of charge via the Internet at http://pubs.acs.org.

JA0667211